# Low-Loss Silicon Photonic 16 × 16 Cyclic AWGR Based on SOI Platform

Rui Huang ⬤, Haiyang Huang ⬤, Yingxuan Zhao ⬤, Yang Li ⬤, XiaoJuan She, Han Liao, Junbo Zhu, Zijian Zhu, Xiang Liu, Hongbao Liu, Zhen Sheng, and Fuwan Gan ⬤

*Abstract*—We experimentally demonstrate a low-loss and low-crosstalk 16-channel 200 GHz-channel-spacing arrayed waveguide grating router (AWGR) with a size of $0.67 \times 0.37$ mm², targeting for C-band wavelength division multiplexing (WDM) interconnect routing applications. As a result, the AWGR features a channel spacing of $200\pm10$ GHz, a free spectral range of 25.62 nm and a 3 dB channel bandwidth of 0.9 nm. Based on comprehensive optimal design, the measured characterization revealed 5.55 dB maximum channel loss non-uniformity with 1.13 dB best-case channel insertion loss. Besides, the fabricated device exhibits good cyclic-frequency operation for all $16 \times 16$ port combinations with channel crosstalk of –15.11 dB.

*Index Terms*—Arrayed waveguide grating router (AWGR), dense-wavelength division multiplexing (DWDM), optical interconnects.

## I. INTRODUCTION

WITH the development of cloud computing and the increasing number of servers, data center (DC) is required to be cost-effective and energy efficient. The optical interconnection density of data center will be expanded by using wavelength division multiplexing (WDM) technology [1]. Arrayed waveguide grating routers (AWGRs) are the key components in dense wavelength division multiplexing (DWDM) with advantages of

broadband and low power consumption. It can provide all-to-all communication among N nodes with N wavelengths simultaneously [2]. In addition to the traditional inter such as rack-scale [3] and board-level interconnects [4], a deeper interconnection can be achieved through on-chip integrated optical technology. Recently, researchers have proposed optical multi-socket board (MSB) architecture [5], following Network-on-Chip (Noc) interconnect [6] based on AWGRs.

AWGRs have been realized in various material platforms. Silica ($SiO_2$) [7] AWGRs have low insertion loss due to the low refractive index contrast. Polymer (Pol) [8] materials have an advantage of low propagation loss in waveguides. AWGR have been developed in Si-nitride (SiN) [9] and Si-oxynitride (SiON) [10] platform which have moderate refractive index contrast. However, these devices cannot be easily integrated with other photonics devices due to their large footprint. For the high refractive index contrast between silicon and silica, the AWGRs based silicon-on-insulator (SOI) waveguide have smaller waveguide bending radius which can help to further reduce the size of the device. Moreover, the fabrication process is compatible with commercial CMOS technology. Recently, Si-based AWGRs with different channel spacing and number of channels have showed good performance [11]–[17]. However, the SOI waveguides used in the array are sensitive to phase errors, resulting in higher crosstalk and larger insertion loss than low-index contrast device. The phase error of the waveguide is related to the waveguide width variation and its correlation length, which are related to the fabrication process. Besides, it is also related to the derivation of the effective respect to the waveguide width, which can be optimized by widening the width of arrayed waveguides [23]. Therefore, by improving the fabrication process and optimizing the width of arrayed waveguide, the phase error and associated crosstalk can be reduced. Therefore, AWGRs based on SOI platform with low loss, low crosstalk and compact footprints have attracted more attention. Wang *et al.* experimentally demonstrated an $8 \times 8$ AWGR with a channel spacing of 400 GHz that showed a crosstalk of -17 dB and insertion loss of 2.92 dB, by using rib waveguides instead of strip waveguides [18].

In this work, we propose and demonstrate a low-loss and low-crosstalk $16 \times 16$ Si-photonic cyclic- AWGR with core size of $0.67 \times 0.37$ mm². The AWGR center wavelengths are aligned to 1550 nm, with $200\pm10$ GHz channel spacing (CS), 0.9 nm 3-dB bandwidth and a free spectral range (FSR) of 25.62 nm. The device features proper cyclic frequency properties

**(a)**

**(b)**

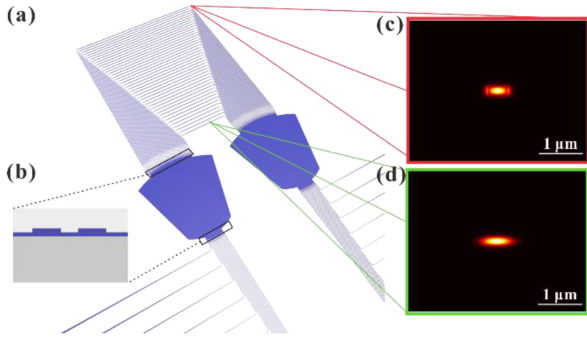**(c)**

1 μm

**(d)**

1 μm



Fig. 1.    (a) Schematic diagram of 16 × 16 200 GHz silicon-based AWGR, (b) 70 nm etch at the boundary of FPR, (c) calculated fundamental TE mode for 450-nm wide bending waveguide; (d) calculated fundamental TE mode for 1-$\mu$m wide arrayed waveguide.



Fig. 2.    Calculated effective index $n_{eff}$ as a function of waveguide width w and its derivative $dn_{eff}/dw$.

for all 16 × 16 port combinations with channel insertion losses ranging from 1.13 dB to 6.68 dB and a maximum insertion loss non-uniformity of 5.55 dB. The low loss is achieved by optimizing the width of arrayed waveguide and shallowly etching the junction area between free propagation region (FPR), arrayed waveguides and input/output waveguides. We adopted a wider arrayed waveguide, and obtained a device with lower loss ensuring lower crosstalk level. However, shallowly etching also strengthens the coupling between the output waveguides, resulting in crosstalk. The channel crosstalk was measured to be −15.11 dB, which is still lower than the majority of the reported devices.

## II. OPERATION PRINCIPLE AND DESIGN

As shown in Fig. 1(a), the AWGR includes two parts: free propagation region (FPR) and an array of waveguides (WGs) with linearly increasing length. The AWGR operation can be described as follows: An optical signal is input to FPR and diffracts. Then the optical components are distributed and transmitted through arrayed waveguide. Due to the length increment of adjacent arrayed waveguides, the optical components gain different delays. Finally, the optical components interfere at the output FPR and are directed to the output waveguides. Optical diffraction and interference that occur in the FPR are the essential principle of an AWG. The grating diffraction equation [19] is:

$$n_s(\lambda)\, d_a \sin \theta_i + n_a(\lambda)\, \Delta L_a + n_s(\lambda)\, d_a \sin\, \theta_o = m\lambda$$

where $n_s(\lambda)$ and $n_a(\lambda)$ are the effective indices of the FPR slabs and arrayed waveguides, respectively. $d_a$ is the pitch of the end of adjacent arrayed waveguides, $\Delta L_a$ is the length increment of adjacent arrayed waveguides, $\theta_i$ is the propagation angle from one of the input waveguides, $\theta_o$ is the propagation angle toward one of the input waveguides, and $m$ is the diffraction order. To realize cyclic wavelengths routing, adjacent diffraction orders should be strictly matched. Therefore, the FSR of the AWG is equal to the product of channel spacing and the channel number,

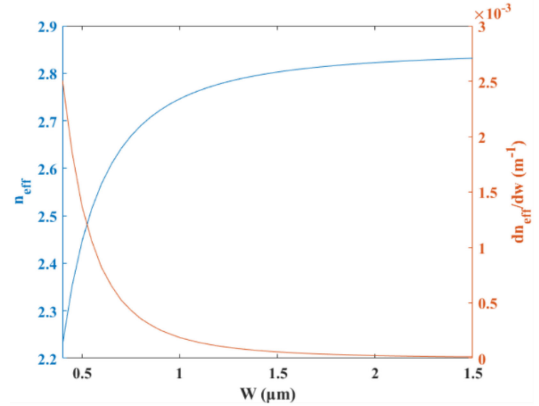$$FSR = \frac{\lambda_c^2}{N_a \Delta L} = N\Delta\lambda$$

where $\lambda_c$ is the center wavelength and $N_a$ is the group refractive index of arrayed waveguides. For N×N AWGR, when the input channel changes, the wavelength response at the output channel makes a cyclic rotation. The performance of the AWGR is usually characterized by the insertion loss and crosstalk in each channel. For AWGRs, low loss is an essential property usually including the material loss, bending loss, waveguide scattering loss and transition loss between the FPR and the arrayed waveguides. In this work, we choose silicon as the material of the AWGR, and the bending radius is set to 5 $\mu$m to obtain a small footprint. Thus, in order to achieve a low-loss AWGR, the waveguide scattering loss and transition loss must be fully optimized.

The scattering loss is dominated by the sidewall roughness of waveguides. Therefore, it can be reduced by improving fabrication technology. On the other hand, the scattering loss also depends on the mode interacts with the sidewalls, which can be optimized by designing the waveguide structure, such as using a nano-scale core layer. But the thickness of the silicon core layer is fixed for mature CMOS process. With the increase of waveguide width, the effective index increases while the increasing rate decrease, as shown in Fig. 2. It can be seen that the increasing rate has been reduced to a lower level when the waveguide width is 1 $\mu$m. If the waveguide width continues to increase, more high-order modes will be excited, which will degrade the loss performance. Based on the above considerations, 1 $\mu$m is a good trad-off to obtain smaller insertion loss. Calculated fundamental TE modes profile for 450 nm and 1 $\mu$m wide waveguide are shown in Fig. 1. It indicates that the mode will be less affected by the sidewalls when the waveguide becomes wider.

The transition loss is also another important part of AWGR on-chip loss, which is mainly due to gaps between the FPR and the arrayed waveguides. It is inversely proportional to gap size but is limited by the fabrication process. In order to reduce transition loss, a double-etched taper is used as mode converter between FPR and arrayed waveguides. A similar approach is using vertical tapers at the junctions [21], but it suffers from fabrication difficulties.

| Parameter | Design |
|---|---|
| Number of channels | 16 |
| Center wavelength | 1550 |
| Channel spacing (nm) | 1.6 |
| Diffraction order | 44 |
| Length increment (μm) | 24.683 |
| Length of FPR (μm) | 154 |
| Pitch of adjacent arrayed WGs (μm) | 2.2 |
| Pitch of adjacent input/output WGs(μm) | 2.4 |
| Number of arrayed WGs | 47 |

The device was fabricated on an SOI wafer with a 220-nm-thick top silicon layer and a 2-μm-thick buried oxide layer. As mentioned earlier, the width of arrayed waveguide is 1 μm to reduce the interaction between mode profiles and the side walls. This method is also effective to reduce the crosstalk because it reduces the sensitivity of the effective refractive index to the sidewall roughness. The waveguides at bends have a width of 450 nm and a bending radius of 5 μm to ensure single-mode transmission and a low propagation loss. Also, we use a 70 nm-deep etched taper which is linearly tapered from 450 nm to 2.0 μm to reduce mode mismatch loss between the waveguide mode and slab mode in FPR region. The depth of 70 is determined by the general process standard. And the waveguide with a width of 450 nm is used to ensure single-mode transmission and a low propagation loss. Reducing waveguide gap also can reduce the transition loss [25]. Therefore, the gap between the tapers is 0.2 μm which is limited by the fabrication process. The detailed design parameters of AWGR are listed in Table I.

In order to evaluate the performance of the device, such as peak IL, center wavelength, loss non-uniformity (defined as the difference between minimum and maximum IL value), the transmission spectrum of input #8 in Fig. 3 is obtained by MATLAB code which is based on a 2D-Kirchhoff diffraction formula. It can be seen that the spectral response is repeated over a wavelength span which is called free spectral range (FSR). The results indicted a CS of 200 GHz and a FSR of 25.6 nm which are consistent with the design. The simulation non-uniformity and crosstalk are 1.83 dB and −30 dB, respectively. The simulated transmission spectral of the device for width variation of 0, ±5 and ±10 nm is shown in Fig. 3. The width variation within ±10 is reasonable for CMOS fabrication process, so the variation of wavelength position can be controlled within 1.6 nm. To better control the wavelength shift, we can adjust the wavelength position through thermal tuning.

## III. FABRICATION AND CHARACTERIZATION

The proposed device was implemented on Semiconductor Manufacturing International Corporation (SMIC). Layout and scanning electron microscope (SEM) images of the fabricated Si AWGR device are shown in Fig. 4. The measured footprint of our device is $1.27 \times 0.37$ mm$^2$ where the core size is $0.67 \times 0.37$ mm$^2$. Besides, the overall size has potential to be optimized
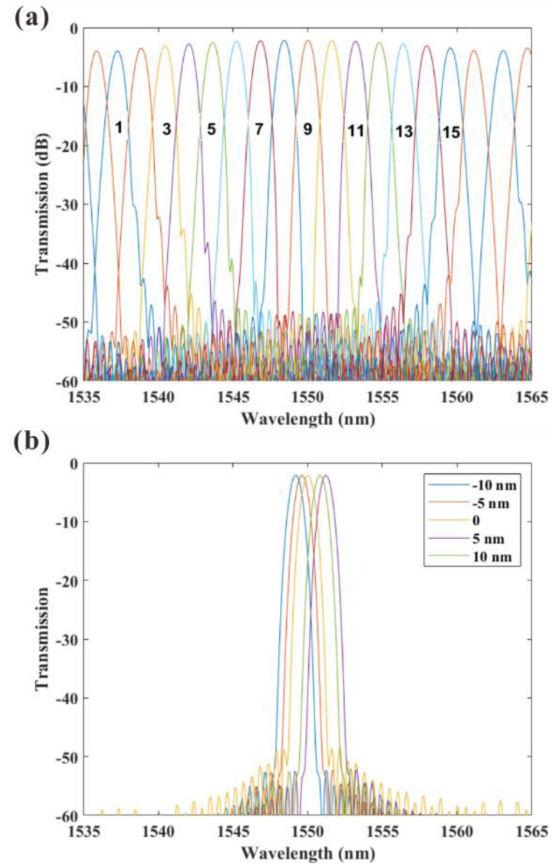


Fig. 3. (a) Simulated transmission spectral of input 8 to all output ports of the 16 × 16 AWGR. The channel spacing and free spectral range are 200 GHz and 25.6 nm respectively. (b) Simulated transmission spectral of input 8 to output #9 with different width variation.
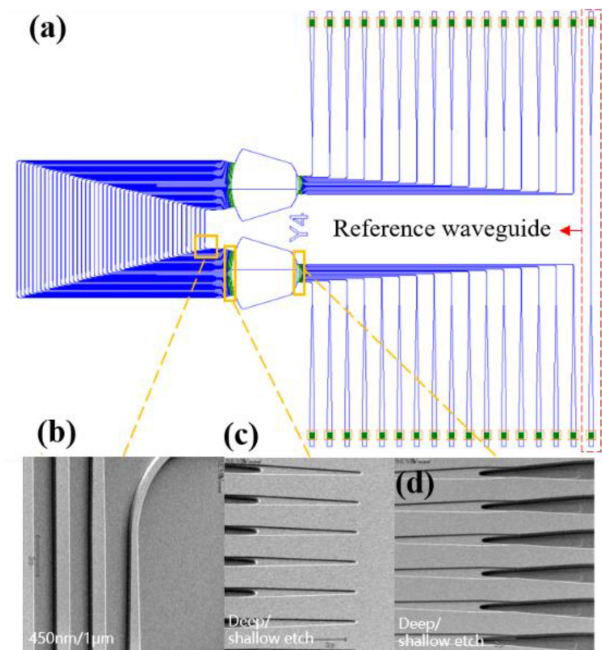


Fig. 4. (a) Layout image of AWGR with a core size of $0.67 \times 0.37$ mm$^2$. SEM images of (a) 1-μm wide arrayed waveguides and 450-nm wide bending waveguides and (c-d) 70 nm etched at the boundary of FPR.
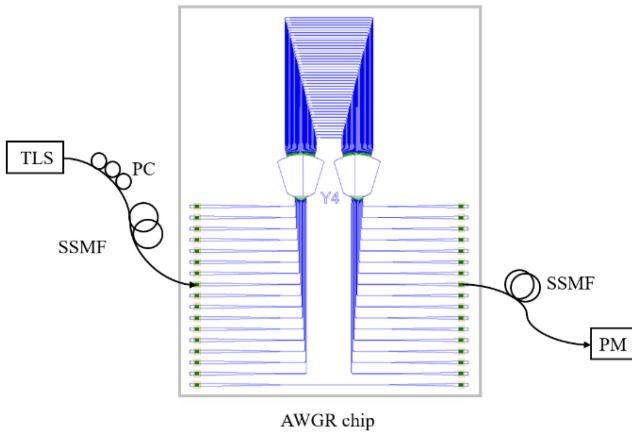
Fig. 5.    The experimental setup for evaluating the transmission characteristics of the Si AWG.
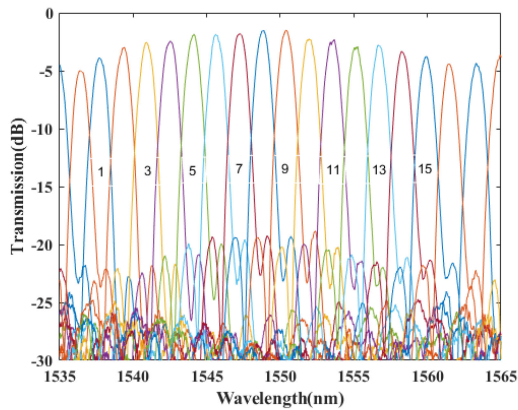


Fig. 7.    The measured spectral response for output channel #8.



Fig. 6.    Measured transmission spectral of input 8 to all output ports of the 16 × 16 AWGR.

by arranging the grating couplers in the width direction [25]. It can be seen that a reference waveguide is fabricated under the device to normalize the spectral responses. The grating coupler, targeting for TE-polarization operation, is used to coupler light into the AWGR at C-band. Fig. 4 show a coupled structure of a 70 nm etched taper near FPR and 220 nm etched waveguide in the array. Pitch of adjoint arrayed waveguide and adjoint output waveguide are 2.2 $\mu$m and 2.4 $\mu$m with 2.0 $\mu$m-wide tapers. The width of bending waveguide is gradually taped from 450 nm to 1um as shown in Fig. 4.

To test the performance of the device, a standard single-mode fiber (SSMF) is used to couple the input light from a tunable laser source (TSL) to the AWGR through grating couplers. A polarization controller (PC) is used to control the polarization to the TE mode. Finally, a power meter (PM) is used to receive the light passing through the AWGR. Fig. 5 show the experimental setup. The loss of reference waveguide is 9.75 dB including the coupling loss and the straight waveguide loss is 0.027 dB.

Fig. 6 shows the normalized transmission spectrum of input #8 to all output ports of the 16 × 16 AWGR in the wavelength range from 1535 nm to 1565 nm. The FSR and CS are 25.62 nm and 200±10 GHz which are very close to the simulated values.
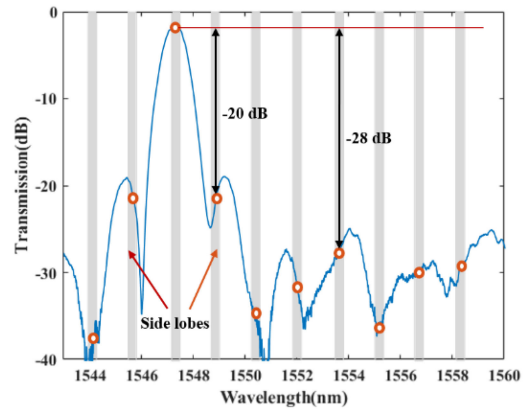
From the normalized responses shown in Fig. 6, it can be seen that the lowest IL of the fabrication AWGR is 1.45 dB, which is mainly due to double-etched tapers and small gaps between arrayed waveguides. The loss non-uniformity is about 2.37 dB due to the Gaussian-shaped far-field distribution of the arrayed waveguides. These data indicate the simulation results match the experiment results.

Fig. 7 shows the measured transmission response of #8 output channel. It can be seen that the cross talk from the adjacent channels is −20 dB while the non-adjacent crosstalk is as low as −28 dB. The experimental results show that there are two side lobes on both sides of the main peak. This is due to the coupling between the output waveguides [20], which was not taken into account in the simulation. In our design, we use 70 nm etched taper to reduce the transition loss between FPR and input/output waveguides as shown in Fig. 4(d). Therefore, the crosstalk can be improved by deep etched output waveguide or widening the gap of adjacent output waveguides.

After normalized to a reference straight waveguide, the measured spectral response of 16 × 200 GHz AWGR is shown in Fig. 8 and revealed cyclic frequency operation. For off-center channels, the crosstalk and the insertion loss increased. The AWGR operating channel mean wavelength value is presented in Fig. 9. A max deviation of 0.44 nm was observed in the measured operating channels compared to the respective mean wavelengths. The discrepancies are the results of phase errors accumulated due to the roughness of arrayed waveguides. The phase error caused by fabrication process variation is mainly cause of wavelength shift. TiN heaters can be used to optimize the wavelength shift [28], [29].

The measured channel peak loss and non-uniformity values of the AWGR are shown in Fig. 10. The horizontal axis represents the input channel, and the vertical axis represents the measured insertion loss of the output channels. The length of the error bars represents the non-uniformity [17]. The channel peak losses are ranged from 1.13 dB to 6.68 dB and the loss non-uniformity is 5.55 dB for all channels. But the peak loss is increased to 3.95 dB because the light is tilted into the FPR region and cannot be fully coupled into the arrayed waveguides. As mentioned above, the
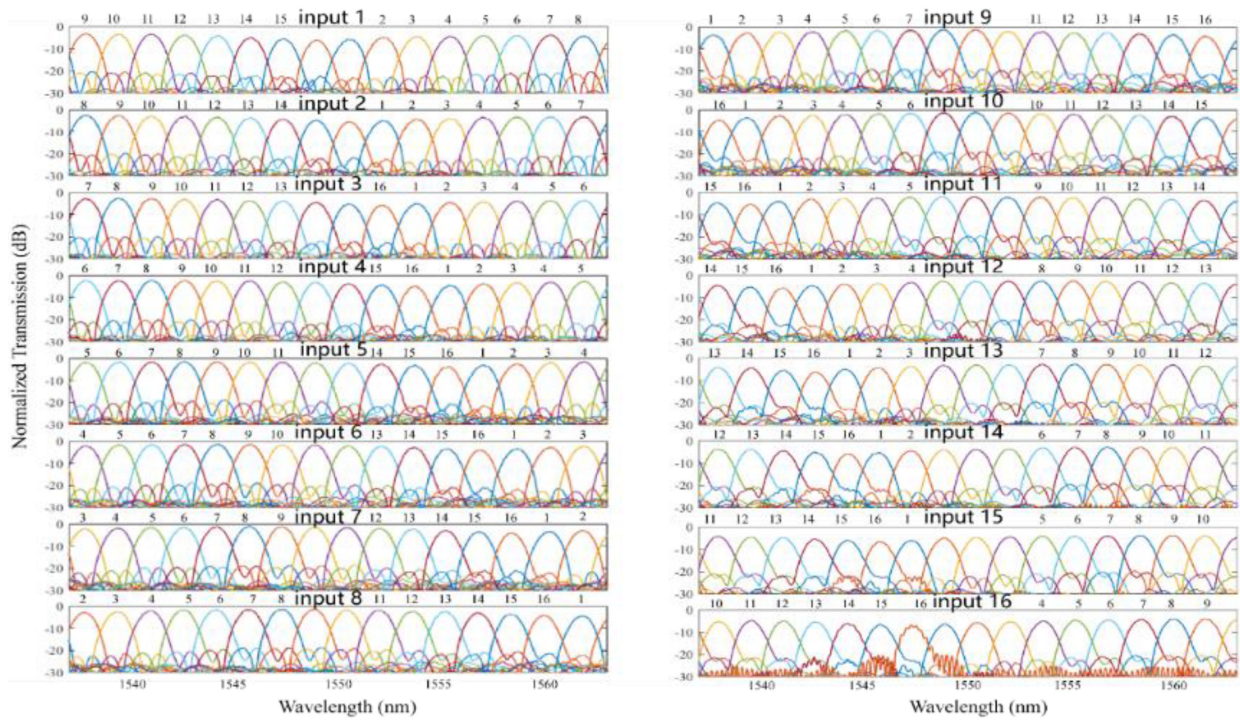
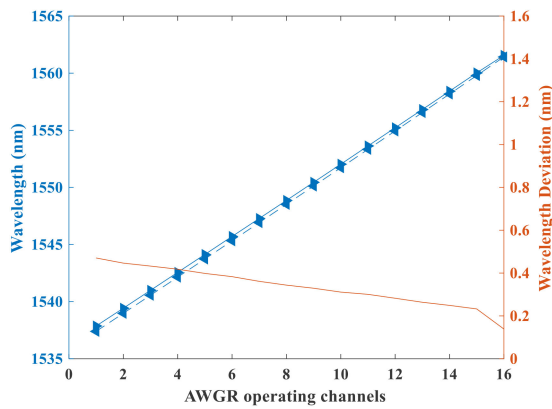Fig. 8. Measured spectral response of the 16 × 16 AWGR.



Fig. 9. Measured wavelength and wavelength deviation between design value. The max wavelength deviation is 0.44 nm.
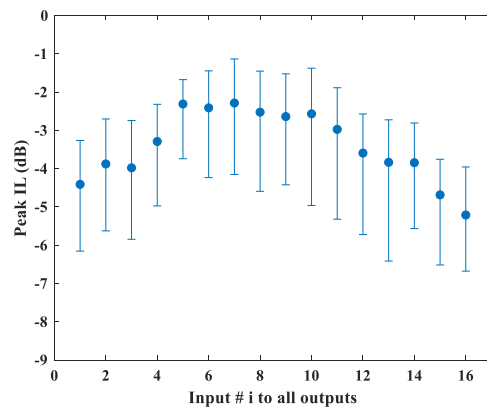


Fig. 10. Measured channel peak insertion loss and uniformity for all Input #i to all output port combinations. The dot means the average loss for all outports. The minimum loss is 1.13 dB and the loss uniformity is 5.55 dB. The length of error bars represents the non-uniformity of insertion loss.

loss is improved by the double-etched taper at the boundary of FPR.

As shown in Fig. 11, it is a heat map with crosstalk values for all Input #i to all output port combinations. The measured crosstalk ranges from −24.45 dB to −15.11 dB. The crosstalk level can reach −24.45 dB for Input #8 to Output #3. The worst-case single channel crosstalk of −15.11 dB is because of the shallow etched tapers between the FPR and the output waveguides. Therefore, crosstalk characteristics can be improved by optimizing the output waveguide structures, such as widen the gap between adjacent tapers or use 220-nm etched tapers. In principle, the output channel with larger channel number and that

with smaller channel numbers are symmetrical, so the spectrum is symmetrical as shown in Fig. 2. We measured different device over different fabrication runs, the variation of the crosstalk level for different output channels is irregular. Therefore, this phenomenon is mainly caused by fabrication variations. The performances of AWGRs on SOI platforms are listed in Table II for comparison. All measures insertion loss and crosstalk in the table are for the center channel. From this comparison, our device has a good performance in terms of both the insertion loss and crosstalk.

TABLE II
COMPARISON BETWEEN STATE-OF-THE-ART AWGRS

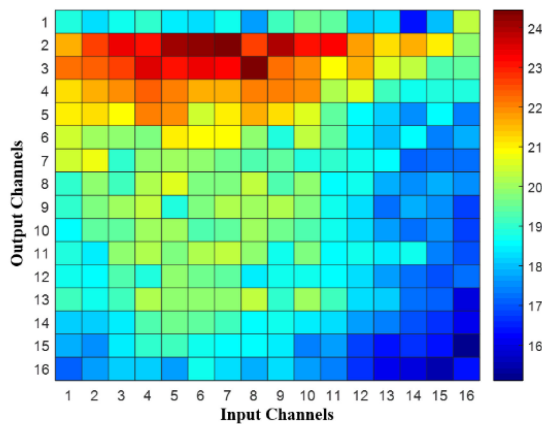| Ref | Channel spacing (GHz) | Channel number | FSR (nm) | Insertion loss (dB) | Crosstalk (dB) | Footprint ($\mu m^2$) |
|---|---|---|---|---|---|---|
| [25] | 250 | 4 | 6 | 3.5 | -12 | 425×125 |
| [26] | 200 | 16 | 25.3 | 2.2 | -17 | 500×200 |
| [12] | 400 | 16 | 51.2 | 3 | -19 | 475×330 |
| [11] | 200 | 16 | 29 | 2 | -22.5 | 920×446 |
| [11] | 400 | 16 | 54 | 1.5 | -26 | 530×435 |
| [22] | 200 | 16 | 24.5 | 3.5 | -16 | 1200×1000 |
| [24] | 200 | 16 | 25.8 | 3 | -16 | - |
| [24] | 400 | 8 | 25.8 | 3 | -18 | - |
| [27] | 200 | 16 | 25.6 | 2.2 | -8 | 580×170 |
| This work | 200 | 16 | 25.62 | 1.45 | -15.11 | 670×370 |



Fig. 11. Heat map with measured crosstalk values for all Input/Output combinations. The crosstalk is about −15.11 dB.

## IV. CONCLUSION

In this paper, we designed and experimentally demonstrated a low-loss 16 × 16 AWGR targeting for C-band DWDM applications on 220 nm-thick SOI platform. The device has a compact core size of $0.67 \times 0.37\,mm^2$. The AWGR shows proper cyclic-frequency operation for all channels, with minimum insertion loss of 1.13 dB. We also obtained a channel spacing of 200±10 GHz and a free spectral range of 25.62 nm. Besides, the crosstalk level is −15.11 dB. The proposed AWGR with good cyclic property and low insertion loss has a great potential in various optical interconnect and optical communications systems.

## REFERENCES

[1] H. Liu, C. F. Lam, and C. Johnson, "Scaling optical interconnects in datacenter networks opportunities and challenges for WDM," in *Proc. 18th IEEE Symp. High Perform. Interconnects*, 2010, pp. 113–116.

[2] S. Cheung, T. Su, K. Okamoto, and S. J. B. Yoo, "Ultra-compact silicon photonic 512 × 512 25 GHz arrayed waveguide grating router," *IEEE J. Sel. Topics Quantum Electron.*, vol. 20, no. 4, pp. 310–316, Jul./Aug. 2014.

[3] M. Moralis-Pegios, N. Terzenidis, G. Mourgias-Alexandris, K. Vyrsokinos, and N. Pleros, "A 1024-port optical uni- and multicast packet switch fabric," *J. Lightw. Technol.*, vol. 37, no. 4, pp. 1415–1423, Feb. 2019.

[4] R. Proietti, Z. Cao, Y. Li, and S. J. B. Yoo, "Scalable and distributed optical interconnect architecture based on AWGR for HPC and data centers," in *Proc. Opt. Fiber Commun. Conf.*, 2014, pp. 1–3, doi: 10.1364/OFC.2014.Th2A.59.

[5] D. R. Yu et al., "A scalable silicon photonic chip-scale optical switch for high performance computing systems," *Opt. Exp.*, vol. 21, no. 26, pp. 32655–32667, 2013.

[6] P. Grani, R. Proietti, S. Cheung, and S. J. B. Yoo, "Flat-topology high-throughput compute node with AWGR-based optical-interconnects," *J. Lightw. Technol.*, vol. 34, no. 12, pp. 2959–2968, Jun. 2016.

[7] N. A. Idris and H. Tsuda, "6.4-THz-spacing, 10-channel cyclic arrayed waveguide grating for T- and O-band coarse WDM," *IEICE Electron. Exp.*, vol. 13, no. 7, pp. 1–7, 2016.

[8] S. Takenobu et al., "All-polymer 8×8 AWG wavelength router using ultra low loss polymer optical waveguide material (CYTOPTM)," in *Proc. Conf. Opt. Fiber Commun./Nat. Fiber Opt. Eng. Conf.*, Feb. 2008, pp. 1–3.

[9] Y. Zhang et al., "Foundry-enabled scalable all-to-all optical interconnects using silicon nitride arrayed waveguide router interposers and silicon photonic transceivers," *IEEE J. Sel. Top. Quantum Electron.*, vol. 25, no. 5, Sep./Oct. 2019, Art no. 8300409.

[10] S. Wang, T. Lang, Y. Wu, and J.-J. He, "16 × 16 AWG router based on silicon oxynitride waveguide platform," in *Proc. CLEO Pacific Rim Conf.*, 2018, pp. 1–2.

[11] S. Pathak et al., "Effect of mask discretization on performance of silicon arrayed waveguide gratings," *IEEE Photon. Technol. Lett.*, vol. 26, no. 7, pp. 718–721, 2014.

[12] S. Pathak, M. Vanslembrouck, P. Dumon, D. Van Thourhout, and W. Bogaerts, "Compact 16×16 channel routers based on silicon-oninsulator AWGs," in *Proc. Annu. Symp. IEEE Photon.*, 2011, pp. 101–104.

[13] G. Song, J. Zou, and J. J. He, "Ultra-compact silicon-arrayed waveguide grating routers for optical interconnect systems," *Chin. Opt. Lett.*, vol. 15, no. 3, 2017, Art. no. 030603.

[14] Y. Wu, T.-N.-T. Lang, J. Song, and J.-J. He, "A 8 × 8 arrayed waveguide grating router based on SOI platform," in *Proc. 16th Int. Conf. Opt. Commun. Netw.*, Aug. 2017, pp. 1–3.

[15] S. Pitris et al., "Silicon photonic 8 × 8 cyclic arrayed waveguide grating router for O-band on-chip communication," *Opt. Exp.*, vol. 26, no. 5, pp. 6276–6284, 2018.

[16] G. Chen, J. Zou, T. Lang, and J. J. He, "Compact 4 × 4 1250 GHz silicon arrayed waveguide grating router for optical interconnects," *Proc. SPIE*, vol. 9367, Feb. 2015, Art. no. 936717.

[17] K. Fotiadis *et al.*, "Silicon photonic 16 × 16 cyclic AWGR for DWDM O-Band interconnects," *IEEE Photon. Technol. Lett.*, vol. 32, no. 19, pp. 1233–1236, Oct. 2020.

[18] J. Wang *et al.*, "Low-loss and low-crosstalk 8 × 8 silicon nanowire AWG routers fabricated with CMOS technology," *Opt. Exp.*, vol. 22, pp. 9395–9404, 2014.

[19] M. K. Smit and C. Van Dam, "PHASAR-based WDM-devices: Principles, design and applications," *IEEE J. Sel. Topics Quantum Electron.*, vol. 2, no. 2, pp. 236–250, Jun. 1996.

[20] D. Dai *et al.*, "Low-loss $Si_3N_4$ arrayed-waveguide grating (de) multiplexer using nano-core optical waveguides," *Opt. Exp.*, vol. 19, no. 15, pp. 14130–14136, 2011.

[21] A. Sugita, A. Kaneko, K. Okamoto, M. Itoh, A. Himeno, and Y. Ohmori, "Very low insertion loss arrayed-waveguide grating with vertically tapered waveguides," *IEEE Photon. Technol. Lett.*, vol. 12, no. 9, pp. 1180–1182, Sep. 2000.

[22] Y. Wu, T. Lang, and J. J. HE, "Horseshoe-shaped 16 × 16 arrayed waveguide grating router based on SOI platform," in *Proc. Asia Commun. Photon. Conf.*, 2017, Paper no. S4J.3.

[23] H. Park, S. K. Kang, J. H. Lee, and S. Lee, "Simplified crosstalk floor representation for a design parameter of silicon AWG," in *Proc. Int. Conf. Opt. Internet*, 2014, pp. 1–2.

[24] D. Kim, J. Lee, J. H. Song, J. Pyo, and G. Kim, "Crosstalk reduction in a shallow-etched silicon nanowire AWG," *IEEE Photon. Technol. Lett.*, vol. 20, no. 19, pp. 1615–1617, Oct. 2008.

[25] P. Dumon *et al.*, "Compact wavelength router based on a silicon-on-insulator arrayed waveguide grating pigtailed to a fiber array," *Opt. Exp.*, vol. 14, no. 2, pp. 664–669, 2006.

[26] W. Bogaerts *et al.*, "Compact wavelength-selective functions in silicon-on-insulator photonic wires," *IEEE J. Sel. Topics Quantum Electron.*, vol. 12, no. 6, pp. 1394–1401, Nov./Dec. 2006.

[27] L. Zhao *et al.*, "16 channel 200 GHz arrayed waveguide grating based on Si nanowire waveguides," *J. Semicond*, vol. 32, no. 2, 2011, Art. no. 024010.

[28] Y. Yang *et al.*, "Thermo-optically tunable silicon AWG with above 600 GHz channel tunability," *IEEE Photon. Technol. Lett.*, vol. 27, no. 22, pp. 2351–2354, Nov. 2015.

[29] P. Yuan *et al.*, "Design and fabrication of wavelength tunable AWGs based on the thermo-optic effect," *Chin. Opt. Lett.*, vol. 16, no. 1, 2018, Art. no. 010601.